energies

MDPI

Article

Analysis and Design of Self-Oscillating Resonant Converters with Loss-Free Resistor Characteristics

Ricardo Bonache-Samaniego, Carlos Olalla *, Hugo Valderrama-Blavi and Luis Martínez-Salamero

Department of Electrical, Electronic, and Automatic Control Engineering (DEEEA), Universitat Rovira i Virgili, 43007 Tarragona, Spain; ricardo.bonache@urv.cat (R.B.-S.); hugo.valderrama@urv.cat (H.V.-B.); luis.martinez@urv.cat (L.M.-S.)

* Correspondence: carlos.olalla@urv.cat; Tel.: +34-977-559-632

Received: 19 June 2020; Accepted: 12 July 2020; Published: 20 July 2020

Abstract: A general approach for the analysis and design of self-oscillating resonant converters is presented in this paper, for a particular class of circuits in which the change of input voltage polarity is caused by the zero-crossings of the input inductor current. The key features of the method are an analytical description in the time-domain of a spiral that eventually converges into an ellipse, and a frequency–domain analysis that explains the behavior of the ellipse as a limit cycle. On a theoretical basis, this class of circuits behaves as loss-free resistors (LFR) because in steady-state the input inductor current is in phase with the first harmonic of the input voltage. The proposed analytical procedure predicts accurately the amplitude and frequency of the limit cycle and justifies the stability of its generation. This accuracy is reflected in the close agreement between the theoretical expressions and the corresponding simulated and measured waveforms. Third and fourth order resonant converters are designed following simple guidelines derived from the theoretical analysis.

Keywords: resonant power converter; resonant conversion; loss-free resistor; self-oscillation; limit cycle; stability; design

1. Introduction

A variable structure system (VSS) is characterized by the change of its physical configuration depending on its internal state. Switching converters are a clear example of VSS because their change of structure and, therefore, the subsequent repetitive sequence of circuits take place when a function of the converter variables attains a certain value. This function usually depends on a combination of the state-variables and an external signal establishing the switching period as, for example, in pulse-width modulated (PWM) converters.

In resonant converters, the change of structure is performed in the input-excitation stage with the aim of generating a square waveform at the input of the resonant tank. As in PWM converters, the corresponding change of polarity is forced in most of the cases by means of an external signal given by the control system setting the frequency of the excitation [1]. Nonetheless, the change of polarity can also be determined by the change of sign of some converter variables, or a function of them, this being the basis of the self-oscillating resonant conversion mode.

Scattered in the literature, this mode has been attained by means of different techniques [2–15], all having in common the change of the input voltage polarity induced by the internal state of the resonant converter. Some of these papers made contributions in the realization of the controller, detailing the driving circuits for self-oscillation [2,4,11–15]. Others focused on the dynamics: using graphical methods in state-plane or in the frequency response plots [3,4,6], with the describing function method [5,7,10], the Hamel locus [9], and/or showing small-signal models [5,8].

Nonetheless, due to the absence of a unified approach in their analysis and the lack of parametric conditions resulting in the desired operation, self-oscillating converters have been relegated to a secondary role in resonant conversion, where the conventional approach is mainly based on frequency and/or phase-modulation, of which a general overview is given in [16,17]. In frequency-based modulation [18–21], the regulation of the power converter is carried out by regulating the switching frequency above or below the resonant frequency point. In phase-shift (or amplitude) modulation [20–25], the activation of the switches of the converter is controlled to regulate the amplitude of the main component at the input of the resonant tank.

A renewed interest for self-oscillating resonant converters has emerged in the last few years due to their relatively simple implementation and their operation being much closer to the resonant frequency than that of conventional resonant converters regardless of changes in the resonant tank or in the load [26–28]. One of the applications that has shown interest in this mode of operation is wireless power transfer, such as in [15], and in a more recent example that combined conventional and self-oscillating control [29].

A self-oscillating parallel resonant converter (SOPRC) using a mechanism for changing the input voltage polarity based on the inductor current sign was analyzed in previous works [30,31] showing that a limit cycle with an oscillating frequency equal to the circuit natural frequency could be generated provided that the Q factor of the resonant tank was above a minimum value of approximately 3.15. Using this design constraint, the trajectories of the two converter configurations were combined to generate a growing spiral in the $i_L - v_C$ phase-plane that eventually became an ellipse when it reached the attraction perimeter of the limit cycle.

The self-oscillation mechanism presented in [30,31] is investigated in this paper in a class of resonant converters characterized by the existence of a series inductor at the input port of the resonant tank as depicted in Figure 1a, where the input voltage has the positive value V_g for $i_L \geq 0$ and the negative value $-V_g$ for $i_L < 0$. The aim of the control law given by the binary signal u is to lead the converter dynamics to the steady-state behavior illustrated in Figure 1b, where it can be observed that the inductor current is in phase with the first harmonic of the input voltage, which confers a resistive behavior on the input port of the resonant tank. Since the rest of the resonant tank is composed of reactive elements, the power absorbed at the input port is totally transferred to the load at the output port. Thus, the resonant tank with this control law can be modelled as a loss-free resistor (LFR) [32–34].

The first goal of the paper is to extend the analytical approach of [30] to 3rd and 4th order resonant converters by explaining the mechanism of limit cycle generation and demonstrating its stability. The study combines time-domain and frequency–domain analyses to justify that a spiral starting from zero initial conditions eventually converges into an ellipse that corresponds to the steady-state behavior of the limit cycle. The second goal is that the design-oriented analysis involved in this study should result in simple design guidelines predicting the steady-state operating point of the converter. The converters considered in the analysis are the series resonant converter (SRC), parallel resonant converter (PRC), plus LCC, LCL, and LCLC resonant converters as depicted in Figure 2. Note that all of them have a series inductor at the input port of the resonant tank in agreement with the definition of the class of resonant converters considered in this study. The presence of second order converters is justified because the analysis of its self-oscillating operation is reviewed and the stability of its associated spiral analyzed in order to facilitate the extension of the analytical procedure to a third and fourth order structures.

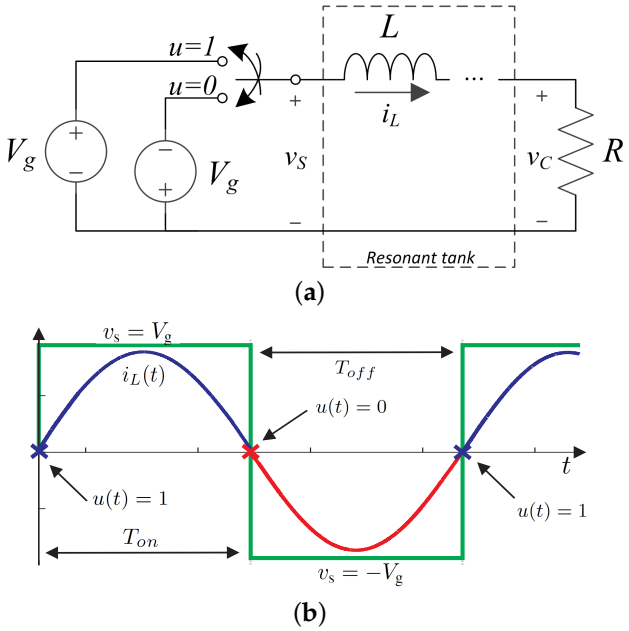

Figure 1. Operating principle of self-oscillating resonant converters with LFR characteristics ($u = 1$ for $i_L \geq 0$, $u = 0$ for $i_L < 0$): (**a**) circuit diagram; (**b**) steady-state waveforms of the input current and the input voltage at the resonant tank.

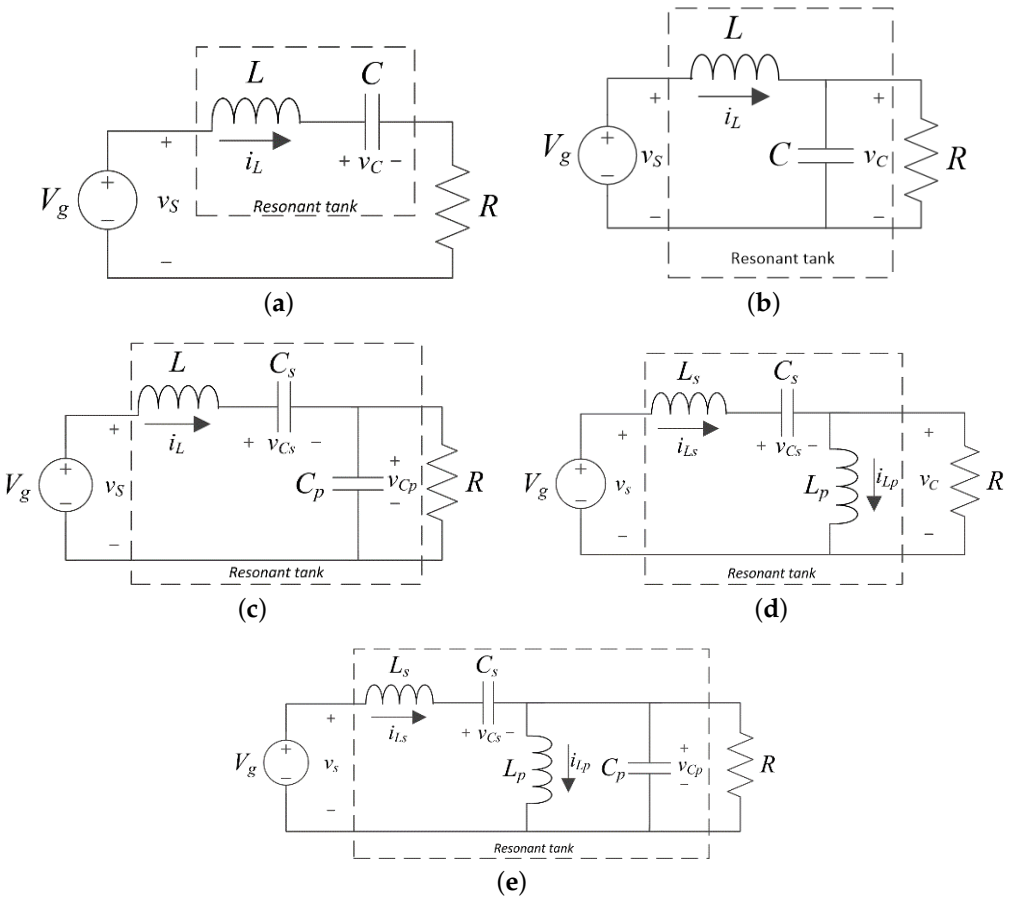

Figure 2. Resonant converters considered in the paper in self-oscillating mode: (**a**) series resonant converter (SRC); (**b**) parallel resonant converter (PRC); (**c**) LCC resonant converter; (**d**) LLC resonant converter; and (**e**) LCLC resonant converter.

This paper is organized as follows: Section 2 reviews the self-oscillating behavior in a parallel resonant converter and introduces the stability analysis of the limit cycle generation by means of a discrete-time recurrence. The generation mechanism of a three-dimensional limit cycle in an LCC resonant converter operating in self-oscillating mode and its corresponding stability are analyzed in Section 3 and verified by experiments. In Section 4, the theoretical predictions of a frequency–domain analysis concerning amplitude and frequency of the different variables associated with the limit cycle in a LCLC resonant converter are verified by simulations. Finally, conclusions are summarized in Section 5.

2. Stability of Self-Oscillating Parallel Resonant Converter

This section describes analytically the self-oscillating mechanism in the PRC by means of a mathematical model of a spiral, which is characterized by a recurrence relating the values of the capacitor voltage after two successive zero-crossings of the inductor current. It has to be pointed out that in [30] the analysis in a generic T_{ON} interval was used to predict the amplitude and frequency of the limit cycle by assuming that the initial and final conditions of the derived transition equation were opposite, i.e., by assuming that the mentioned interval was a semi-cycle of the limit cycle. Therefore, it was not proved that starting from zero initial conditions the growing spiral describing the self-oscillating mechanism converged into an ellipse, which would have justified the stability of the waveform generation.

Now, the objective of the analysis is to justify the stability of the self-oscillation by means of a procedure that can be extended to high order converters.

The phase trajectories of T_{ON} and T_{OFF} states in the PRC (Figure 2b) were combined in [30] to generate a growing spiral that started from the origin of the phase-plane $v_C - i_L$ and eventually reached the attractive perimeter of the limit cycle. The control law established T_{ON} and T_{OFF} state operations for $i_L \geq 0$ and $i_L < 0$, respectively.

As it was demonstrated in that work, the capacitor voltage in a PRC under conditions of underdamped behavior can be expressed for T_{ON} state during a generic interval $t_2 < t < t_3$ and initial conditions $v_C(t_2) = -v_{C_{2n}}$ and $i_L(t_2) = 0$ as follows:

$$v_C(\tau) = e^{-\xi\omega_0\tau}\left\{(-v_{C_{2n}} - V_g)\cos\omega_d\tau - \frac{(-v_{C_{2n}} + V_g)}{2RC\omega_d}\sin\omega_d\tau\right\} + V_g \tag{1}$$

where $\tau = t - t_2$, $\omega_d = \omega_o\sqrt{1-\xi^2}$, ω_o and ξ being respectively the natural oscillation frequency and the damping factor given by $\omega_o = \frac{1}{\sqrt{LC}}$ and $\xi = \frac{\sqrt{LC}}{2CR}$.

Equation (1) has its maximum value $v_{C_{2n+1}}$ at instant τ_C given by

$$\omega_d\tau_c = \tan^{-1}\left(-\frac{2\xi\sqrt{1-\xi^2}v_{C_{2n}}}{V_g + v_{C_{2n}}(1-2\xi^2)}\right) + \pi \tag{2}$$

$$v_{C_{2n+1}} = e^{-\xi\omega_0\tau_c}\sqrt{V_g^2 + {v_{C_{2n}}}^2 + 2V_g v_{C_{2n}}(1-2\xi^2)} + V_g \tag{3}$$

Under conditions of large Q, it is apparent that $\xi << 1$, or equivalently, $1 - 2\xi^2 \approx 1$ and $\omega_d \approx \omega_0$, so that Equations (2) and (3) become

$$\omega_0\tau_c \approx \tan^{-1}\left(-\frac{2\xi v_{C_{2n}}}{V_g + v_{C_{2n}}}\right) + \pi \approx \pi \tag{4}$$

$$v_{C_{2n+1}} = e^{-\xi\pi}(V_g + v_{C_{2n}}) + V_g \tag{5}$$

Equation (5) is a recurrence describing the transition from the initial point of a generic branch of the spiral to its final point for the corresponding T_{ON} interval as depicted in Figure 3. A similar analysis for a generic T_{OFF} interval will result in

$$-v_{C_{2n+2}} = e^{-\xi\pi}(-V_g - v_{C_{2n+1}}) - V_g \tag{6}$$

Introducing (5) into (6) yields the mathematical description of the spiral for a complete cycle

$$\begin{aligned} -v_{C_{2n+2}} &= e^{-\xi\pi}(-2V_g - e^{-\xi\pi}V_g - e^{-\xi\pi}v_{C_{2n}}) - V_g \\ &= -V_g(1+e^{-\xi\pi})^2 - v_{C_{2n}}e^{-2\pi} \end{aligned} \tag{7}$$

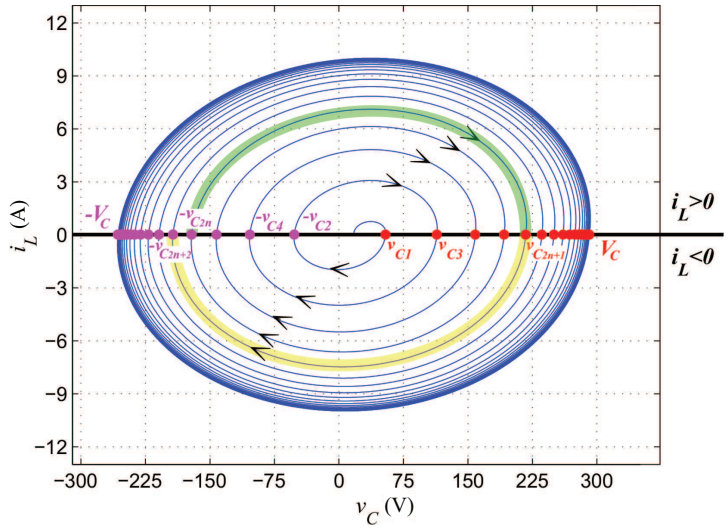

Figure 3. Matlab simulation of the self-oscillating PRC trajectory in the phase plane $v_C - i_L$ for $C = 10.5$ nF, $L = 8$ µH, R = 400 Ω, $V_g = 20$ V. The green branch corresponds to a generic T_{ON} interval.

It can be observed that (7) describes a stable system since the term multiplying $v_{C_{2n}}$ is less than unity.

On the other hand, if n is the n-th cycle of the spiral, recurrence (7) for $n = 1$ will describe the transition from $-v_{C2}$ to $-v_{C4}$ as follows:

$$-v_{C4} = G - v_{C2}r \tag{8}$$

where $G = -V_g(1+e^{-\xi\pi})^2$ and $r = e^{-2\pi}$. After n cycles:

$$-v_{C_{2n+2}} = (G + Gr + Gr^2 + ... + Gr^{n-1}) - v_{C2}r^n \tag{9}$$

Therefore,

$$\lim_{n\to\infty} v_{C_{2n+2}} = \frac{G}{1-r} = \frac{V_g(1+e^{-\xi\pi})^2}{1-e^{-2\xi\pi}} = \frac{V_g(1+e^{-\xi\pi})}{1-e^{-\xi\pi}} \tag{10}$$

Equation (10) gives the value of the amplitude of the limit cycle, which corresponds to the negative excursion $-V_C$ in Figure 3 and coincides with the value derived in [30] by assuming the recurrence in Equation (5) in the limit cycle, i.e., considering symmetric excursions for the capacitor voltage, so that $v_{C_{2n+1}} = v_{C_{2n}}$.

Finally, the period of the limit cycle will be given by

$$T = \frac{2\pi}{\omega_0} \tag{11}$$

which is the equation derived in [30] assuming symmetry conditions in the transition equation describing a generic T_{ON} interval.

3. 3rd Order Self-Oscillating Resonant Converters

The application of the previous approach to a SRC resonant converter (Figure 2a) is straightforward, but its extension to third order converters is more complex because it involves the analytical description of a three-dimensional spiral. However, this difficulty can be overcome by analyzing the spiral projection in two phase-planes, each of them associated with the input inductor current and one of the remaining state variables. This idea is illustrated in Figure 4 for the LCC resonant converter (Figure 2c), where the three-dimensional spiral in Figure 4a is projected in the phase planes $i_L - v_{Cp}$ and $i_L - v_{Cs}$ in Figure 4b,c respectively. The problem is thus reduced to obtaining the corresponding recurrences describing the limit cycle generation in Figure 4b,c.

Deriving both recurrences requires obtaining first the characteristic polynomial of the system. As in the PRC case, the analysis of the converter in a generic T_{ON} interval is performed next with the aim of obtaining the duration of the interval. The hypothesis of large separation between the real parts of the converter poles allows solving the equation of the interval duration. The particularization of the obtained generic interval equation to the T_{ON} interval of the limit cycle leads to the amplitude of the converter signals in steady-state. The subsequent hypothesis of large Q associated with the parallel capacitor yields the equation of the oscillation frequency of the limit cycle and facilitates the identification of the rest of the parameters. The corollary of this analysis in both time and frequency domains is a simple design procedure and a discrete-time model that justifies the unconditional stability of the self-oscillation.

3.1. Characteristic Polynomial

In the LCC resonant converter shown in Figure 2c, transfer functions $H(s)$ and $Y(s)$ relating respectively input to output voltage and input voltage to inductor current (input admittance) are given by

$$H(s) = \frac{V_{Cp}(s)}{V_{in}(s)} = \frac{\frac{s}{LC_p}}{s^3 + \frac{s^2}{RC_p} + \frac{C_s+C_p}{LC_sC_p}s + \frac{1}{LC_sC_pR}} \tag{12}$$

$$Y(s) = \frac{I_L(s)}{V_{in}(s)} = \frac{\frac{1}{LC_pR}s(C_pR\,s+1)}{s^3 + \frac{s^2}{RC_p} + \frac{C_s+C_p}{LC_sC_p}s + \frac{1}{LC_sC_pR}} \tag{13}$$

From now onwards, it is assumed that the poles of the system consist of one negative real pole and two complex conjugates poles with negative real part, due to the passive nature of the circuit. Under this assumption,

$$s^3 + \frac{s^2}{RC_p} + \frac{C_s+C_p}{LC_sC_p}s + \frac{1}{LC_sC_pR} = (s+\alpha)(s^2 + 2\xi\omega_0 s + \omega_0^2) \tag{14}$$

can be written.

3.2. Analysis in a Generic T_{On} Interval

Assuming that the converter is in a T_{ON} interval with initial conditions $v_{Cs}(t_j) = -V_{Cs_{2n}}$, $i_L(t_j) = 0$, $v_{Cp}(t_j) = -V_{Cp_{2n}}$, where t_j is the initial instant of such interval, then the input voltage will be $v_{in}(t) = V_g$, and therefore the equation of the series capacitor voltage will be given by

$$v_{Cs}(\tau) = Ae^{-\alpha\tau} + Be^{-\xi\,\omega_0\,\tau}\sin\,\omega_d\tau + Ce^{-\xi\,\omega_0\,\tau}\cos\omega_d\tau + V_g \tag{15}$$

where $\omega_d = \omega_0\sqrt{1-\xi^2}$, $\tau = t - t_j$ and A, B, C are constants corresponding to the solution of the homogeneous differential equation of the system.

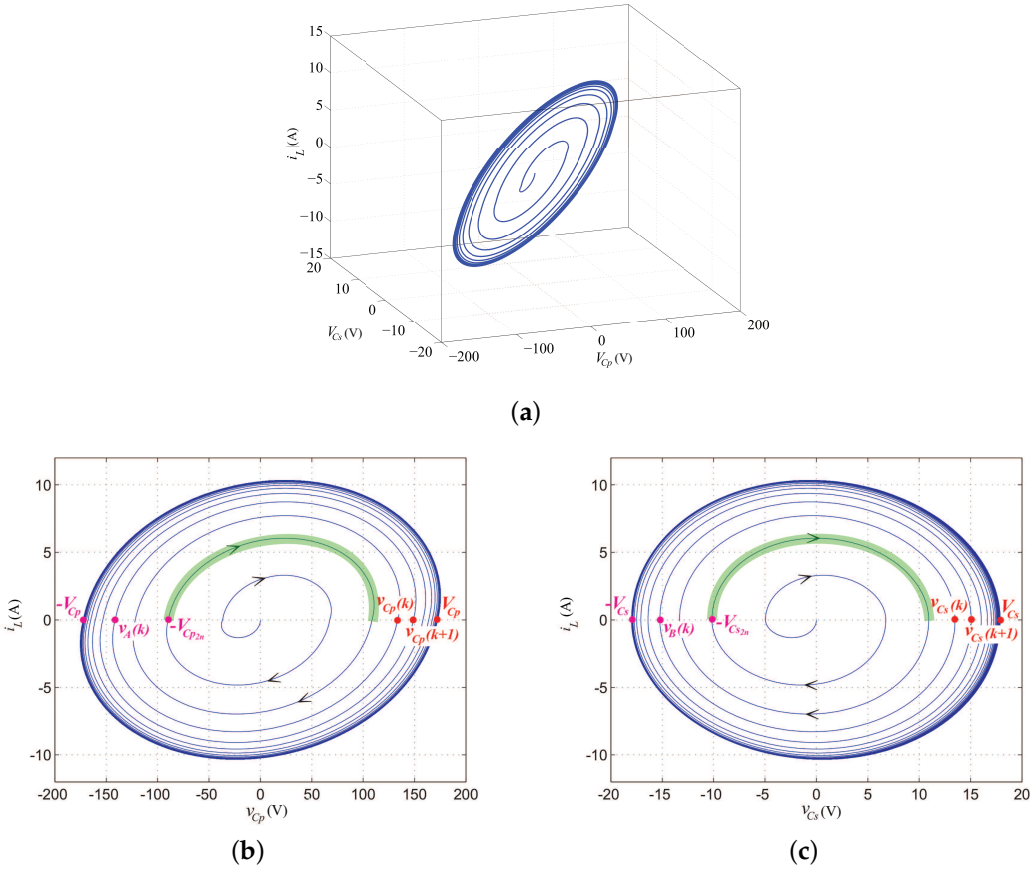

Figure 4. Matlab simulation of the self-oscillating mechanism in the LCC resonant converter under the following conditions. V_g = 24 V, L = 16 µH, C_s = 500 nF, C_p = 50 nF, R = 100 Ω. The green branches represent generic T_{ON} intervals: (**a**) Three dimensional trajectory; (**b**) projection in the phase-plane $i_L - v_{Cp}$; (**c**) projection in the phase-plane $i_L - v_{Cs}$.

On the other hand, since $v_L(t) = L\,di_L/dt$ and $i_L(t) = C_s\,dv_{Cs}/dt$, the inductor current and voltage can be expressed as follows:

$$i_L(\tau) = -C_s A\alpha e^{-\alpha\tau} - C_s e^{-\xi\omega_0\tau}(B\xi\omega_0 + C\omega_d)\,\sin\omega_d\tau + C_s e^{-\xi\omega_0\tau}(B\omega_d - C\xi\omega_0)\cos\omega_d\tau \tag{16}$$

$$\begin{aligned} v_L(\tau) =& LC_s A\alpha^2 e^{-\alpha\tau} + (-2LC_s\,B\,\xi\,\omega_0\,\omega_d + LC_s C\xi^2\omega_0^2 - LCC_s\omega_d^2)e^{-\xi\omega_0\tau}\cos\omega_d\tau \\ &+ (LC_s B\xi^2\omega_0^2 - LC_s B\omega_d^2 + 2LC_s C\xi\omega_d\omega_0)e^{-\xi\omega_0\tau}\sin\omega_d\tau \end{aligned} \tag{17}$$

Moreover, voltages in the circuit are related by

$$v_{Cp}(t) = V_g - v_{Cs}(t) - v_L(t) \tag{18}$$

At the beginning of the interval, i.e., $t = t_j$, or equivalently at $\tau = 0$, it can be written:

$$\frac{dv_{Cs}(0)}{dt} = \frac{i_L(0)}{C_s} = 0 \tag{19}$$

Particularizing Equations (15)–(19) at $\tau = 0$ results in the following set of equations relating constants A, B, C with the initial conditions of the interval and circuit parameters

$$\begin{pmatrix} 1 & 0 & 1 \\ -\alpha & \omega_d & -\xi\,\omega_0 \\ \alpha^2 & -2\xi\,\omega_0\,\omega_d & \omega_0^2\,(2\xi^2-1) \end{pmatrix} \begin{pmatrix} A \\ B \\ C \end{pmatrix} = \begin{pmatrix} -V_g - V_{Cs_{2n}} \\ 0 \\ \frac{V_g + V_{Cs_{2n}} + V_{Cp_{2n}}}{LC_s} \end{pmatrix} \tag{20}$$

Solving the previous set of equations leads to:

$$A = \frac{1}{\Delta}\left((V_g + V_{Cs_{2n}})\,\omega_0^2 - \frac{V_g + V_{Cs_{2n}} + V_{Cp_{2n}}}{LC_s} \right) \tag{21}$$

$$B = \frac{1}{\omega_d \Delta}\left(\begin{array}{l} \frac{V_g + V_{Cs_{2n}} + V_{Cp_{2n}}}{LC_s}(\xi\omega_0 - \alpha) \\ +\,(V_g + V_{Cs_{2n}})\omega_0\alpha(\xi\alpha - 2\xi^2\omega_0 + \omega_0) \end{array} \right) \tag{22}$$

$$C = \frac{1}{\Delta}\left(\begin{array}{l} \frac{V_g + V_{Cs_{2n}} + V_{Cp_{2n}}}{LC_s} \\ -\,(V_g + V_{Cs_{2n}})(2\xi\omega_0\alpha - \alpha^2) \end{array} \right) \tag{23}$$

where $\Delta = \omega_d\left[2\xi\omega_0\alpha - \alpha^2 - {\omega_0}^2\right]$.

In addition, the T_{ON} interval will end at instant τ_0 for which $i_L(\tau_0) = 0$. Taking into account (16), the following equation is derived:

$$A\alpha e^{-\alpha\tau_0} = e^{-\xi\omega_0\tau_0}\left((B\xi\omega_0 + C\omega_d)\,\sin\,\omega_d\tau_0 + (B\omega_d - C\xi\omega_0)\cos\omega_d\tau_0\right) \tag{24}$$

Now, in order to find the value of τ_0 satisfying Equation (24), it is assumed that the time constant associated with α is much bigger than the time constant associated with $\xi\omega_0$, i.e., α is the dominant pole of the system. This implies that the term $Ae^{-\alpha\tau}$ will be practically constant along the generic T_{ON} interval, and therefore its time derivative will be zero in such interval. Note that this fact is equivalent to impose $\alpha = 0$ in (19)–(24). Hence, (24) can be expressed as follows:

$$e^{-\xi\omega_0\tau_0}\left((B\xi\omega_0 + C\omega_d)\,\sin\,\omega_d\tau_0 + (B\omega_d - C\xi\omega_0)\cos\omega_d\tau_0\right) = 0 \tag{25}$$

whose solution is

$$\omega_d\tau_0 = tg^{-1}\left(\frac{C\xi\omega_0 - B\omega_d}{B\xi\omega_0 + C\omega_d}\right) + \pi. \tag{26}$$

This is equivalent to

$$\omega_d\tau_0 = \pi. \tag{27}$$

3.3. Obtaining the Signal Amplitude in the Limit Cycle

Assuming now that τ_0 is the duration of T_{ON} interval in the limit cycle, we can write $v_{Cs}(\tau_0) = V_{Cs}$ and $v_{Cp}(\tau_0) = V_{Cp}$ due to the symmetry of the limit cycle associated with the phase-planes $i_L - v_{Cs}$ and $i_L - v_{Cp}$ respectively (Figure 4b,c). Hence,

$$v_{Cs}(\tau_0)|_{\alpha=0} = Ae^{-\alpha\tau_0}\big|_{\alpha=0} + B|_{\alpha=0}e^{-\xi\pi}\sin\,\pi + C|_{\alpha=0}e^{-\xi\pi}\cos\pi + V_g = V_{Cs} \tag{28}$$

From (21)–(23) and (28), it follows that

$$V_g(1 + e^{-\xi\pi}) = V_{Cs}(2LC_s\omega_0^2 - 1 - e^{-\xi\pi}) - V_{Cp}(1 + e^{-\xi\pi}) \tag{29}$$

Note that $v_{Cs}(\tau_0) = V_{Cs}$ and $v_{Cp}(\tau_0) = V_{Cp} = V_g - v_{Cs}(\tau_0) - v_L(\tau_0)$. Therefore, $v_L(\tau_0)$ is given by:

$$v_L(\tau_0)|_{\alpha=0} = 2LC_s\xi\omega_0\omega_d B|_{\alpha=0}e^{-\xi\pi} + LC_s C|_{\alpha=0}e^{-\xi\pi}(\omega_d^2 - \xi^2\omega_0^2) \tag{30}$$

Assuming a very small damping factor $\xi << 1$ allows for equating the natural oscillation frequency ω_0 and the damped natural oscillation frequency ω_d. Under this assumption and considering (21)–(23) and (30), the relationship linking the input and the capacitor voltages is as follows:

$$V_g(1 + e^{-\xi\pi}) = V_{Cs}(1 - e^{-\xi\pi}) + V_{Cp}(1 - e^{-\xi\pi}) \tag{31}$$

Solving the set of Equations (29) and (31) results in the capacitor voltage amplitudes of the limit cycle:

$$V_{Cs} = \frac{V_g(1 + e^{-\xi\pi})}{LC_s\omega_0^2(1 - e^{-\xi\pi})} \tag{32}$$

$$V_{Cp} = \frac{V_g(1 + e^{-\xi\pi})(LC_s\omega_0^2 - 1)}{LC_s\omega_0^2(1 - e^{-\xi\pi})} = V_{Cs}(LC_s\omega_0^2 - 1). \tag{33}$$

3.4. Determining the Oscillation Frequency of the Limit Cycle

The difference of magnitude between the time constants has allowed us to establish the duration τ_0 of a generic T_{ON} interval. The subsequent particularization in the case of the limit cycle, i.e., the assumption that the duration of T_{ON} and T_{OFF} intervals are equal, due to the cycle symmetry, allows us to conclude that the period of the limit cycle is $2\tau_0$ and that the angular oscillation frequency is the damped natural oscillation ω_d. In addition, the hypothesis of small damping factor has finally led to equate the damped natural oscillation frequency and the natural oscillation frequency ω_0. Now, the frequency for which the input impedance exhibits a resistive behavior will be determined in order to express the limit cycle oscillation frequency in terms of the circuit parameters.

From (13), the equation of the input impedance is derived

$$Z_{in}(s) = \frac{1}{Y(s)} = \frac{LRC_pC_ss^3 + LC_ss^2 + R(C_s + C_p)s + 1}{C_s(1 + RC_ps)s} \tag{34}$$

Particularizing (34) in $s = j\omega_0$ yields

$$Z_{in}(j\omega_0) = \frac{-jLRC_pC_s{\omega_0}^3 - LC_s{\omega_0}^2 + jR(C_s + C_p)\omega_0 + 1}{jC_s(1 + jRC_p\omega_0)\omega_0} \tag{35}$$

Assuming that natural oscillation frequency ω_0 is given by

$$\omega_0 = \sqrt{\frac{C_s + C_p}{LC_sC_p}} \tag{36}$$

Equation (35) becomes

$$Z_{in}(j\omega_0) = \frac{-1}{jC_p\omega_0(1 + jRC_p\omega_0)} \tag{37}$$

If the parameters fulfill the following condition

$$RC_p\omega_0 >> 1\,, \tag{38}$$

the input impedance will be resistive:

$$Z_{in}(j\omega_0) = \frac{1}{{RC_p}^2{\omega_0}^2} \tag{39}$$

Similarly, introducing condition (38) in (12) yields

$$H(j\omega_0) = -jRC_p\omega_0 \tag{40}$$

Under these conditions, if the input voltage is approximated by its first harmonic, i.e., $v_{in}(t) \approx v_{in1}(t) = V_m \cos\omega_0 t$, where $V_m = 4V_g/\pi$, the equations of inductor current and parallel capacitor voltage will be given by

$$i_L(t) = V_m \frac{RC_p(C_s + C_p)}{LC_s} \cos\omega_0 t \tag{41}$$

$$v_{Cp}(t) = V_m\, \omega_0 C_p\, R\, \sin\, \omega_0 t \tag{42}$$

From (41) and (42), it can be concluded that the LCC behavior under these conditions is similar to that of PRC at the resonant frequency.

It can be observed that condition (38) allows considering that the capacitors are connected in series, so that their respective voltages are proportional, i.e., they are in phase.

$$v_{Cs}(t) = \frac{C_p}{C_s} v_{Cp}(t) = V_m \omega_0 \frac{{C_p}^2}{C_s} R\, \sin\, \omega_0 t \tag{43}$$

It can be also verified that the maximum value of Equation (43) coincides with (33).

3.5. Identifying Parameters α and ξ

Identifying in (14) the coefficients of the third order polynomial results in the following set of equations:

$$\frac{1}{RC_p} = 2\xi\omega_0 + \alpha \tag{44}$$

$$\frac{C_s + C_p}{LC_sC_p} = \omega_0^2 + 2\xi\omega_0\alpha \tag{45}$$

$$\frac{1}{LRC_sC_p} = \alpha\omega_0^2 \tag{46}$$

Fulfilling simultaneously (36) and (45) implies that constraint $\omega_0 >> 2\xi\alpha$ must be satisfied. Hence, (46) can be rewritten as

$$\alpha = \frac{1}{R(C_s + C_p)} \tag{47}$$

From (44) and (47), the following holds

$$2\xi\omega_0 = \frac{C_s}{C_p} \frac{1}{R(C_s + C_p)} = K_C\alpha\,, \tag{48}$$

where $K_C = \frac{C_s}{C_p}$, or equivalently

$$\xi\omega_0 = \frac{K_C\alpha}{2} \tag{49}$$

Equation (49) shows that the hypothesis of large separation between time constants previously employed in the calculation of τ_0 is valid provided that the ratio K_C between the capacitances is large enough. Finally, the damping factor will be expressed by

$$\xi = \frac{K_C}{2(K_C + 1)RC_p} \sqrt{\frac{K_C LC_p}{K_C + 1}} \tag{50}$$

3.6. Converter Design, Simulation, and Experimental Results

Deriving an accurate expression of the generation mechanism of the limit cycle has required an appropriate combination of frequency and time domain analyses with adequate parametric constraints. Now, it will be shown that the converter design is very simple in spite of the apparent complexity of the mentioned analyses.

3.6.1. Converter Design

The converter design is reduced to an appropriate choice of the resonant tank elements according to the following steps:

1. Define the values of input voltage V_g and the amplitude of the output voltage in steady-state V_{Cp}.
2. Define the desired switching frequency ω_0 and the load R.
3. Calculate $Q = V_{Cp}/V_g$.
4. Verify that $Q \gg 1$ holds.
5. Calculate the value of the parallel capacitance with $C_p = \frac{Q}{\omega_0 R}$.
6. Select $K_C \geq 8$ ($K_C = C_s/C_p$) and calculate the value of the series capacitor with $C_s = K_C C_p$.
7. Derive the value of the inductance with $L = \frac{1+K_C}{\omega_0^2 K_C C_p}$.

It is worth remarking that the LCC has been extensively used in electronic ballasts for lamps. In such application, the impedance of the lamp is variable and, in such case, the design should take into account the minimum real impedance of the load as R, which typically corresponds to the value in steady-state operation.

3.6.2. Simulation Results

Figure 5 corroborates the validity of the previous design procedure by means of a PSIM simulation for the following set of parameters and specifications: $V_{Cp} = 180$ V, $V_g = 24$ V, $f_0 = 190$ kHz, $R = 100\,\Omega$, $Q = 6$, $K_C = 10$, $L = 16\,\mu$H, $C_p = 50$ nF and $C_s = 500$ nF. The roots of the characteristic polynomial (14) provided by Matlab for the previous set of parameters are located in $-18,200$ and -90, $9 \times 10^3 \pm j\,1167$, 7×10^3 rads/s, which is in perfect agreement with the values predicted by Equations (36), (47) and (50). In addition, from the observation of the waveforms of Figure 5, it can be deduced that the oscillation frequency is $f_0 = 187$ kHz, i.e., $\omega_0 = 11.7 \times 10^5$ rad/s, which is exactly the value predicted by equation (47). The maximum values of voltages V_{Cs} and V_{Cp} are in Figure 5 $V_{Cs} = 18$ V and $V_{Cp} = 180$ V, which coincides with the values predicted by (32) and (33) respectively as well as with those provided by (42) and (43) correspondingly. Note that voltages in both capacitors are proportional as predicted by the analysis in Section 3.4.

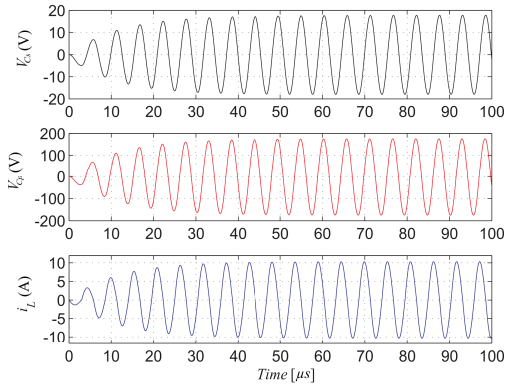

Figure 5. PSIM simulation of the inductor current and capacitor voltage waveforms in the self-oscillating LCC starting from zero initial conditions.

3.6.3. Experimental Results

An experimental prototype of the LCC resonant converter has been implemented taking into account the set of parameters employed in the simulations of Figures 4 and 5, and a controller based on the sign of the inductor current. Figure 6 shows the scheme of the implemented prototype, wherein the power stage consists of an H-bridge connected to a resonant tank. The bridge uses four MOSFETs (IPB200N15N3) activated by two driver ICs UCC27211. The sign of the inductor current, which is sensed by a current transformer, is used to switch the branches of the H-bridge. A picture of the converter and the laboratory stand is shown in Figure 7.

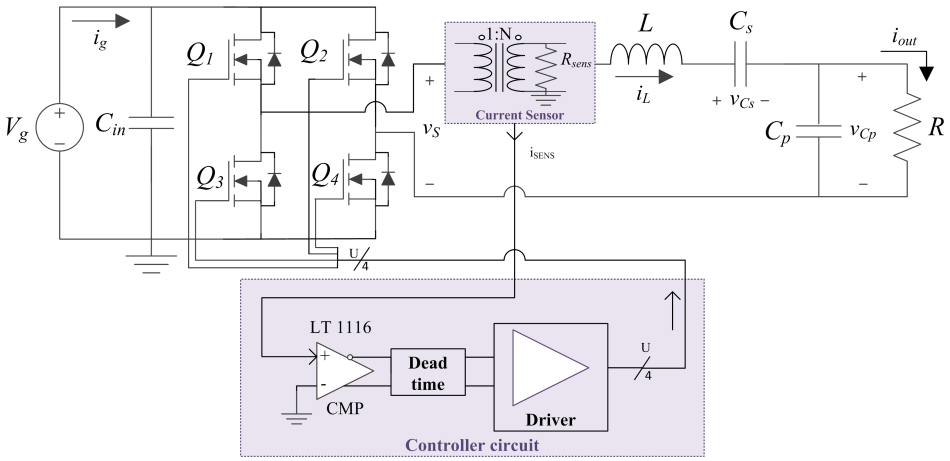

Figure 6. Circuit scheme of the implemented self-oscillating LCC converter.

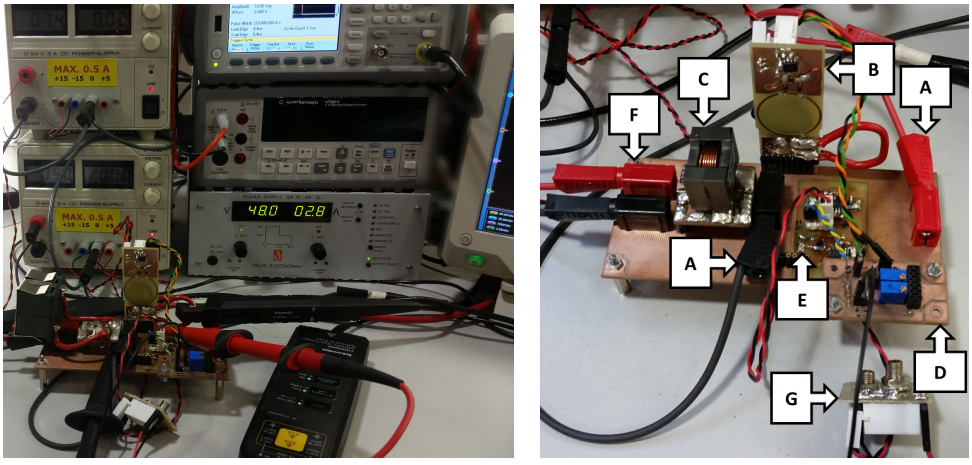

(**a**) (**b**)

Figure 7. Detail of the experimental setup: (**a**) Picture of the laboratory workbench; (**b**) parts of the converter prototype: (A) DC input (two connectors), (B) Current sensor, (C) Resonant tank (LCC), (D) Dead-time circuit, (E) Driver circuit, (F) AC output, (G) activation relay.

Figure 8a shows the steady-state waveforms of current and output voltage of the LCC resonant converter in self-oscillating operation. The circuit exhibits an oscillation frequency of 180 kHz generating an output voltage of 175 V and supplying 130 W to the load. Figure 8b illustrates the corresponding generation of the limit cycle. The propagation delay has been mitigated by selecting a high-speed driver and a relatively low switching frequency, which results in a 70 ns delay not impacting on the converter performance. In addition, the delay effect can be compensated by the use of appropriate networks as it has been recently reported in the design of a 6.78 MHz self-oscillating resonant converter [35].

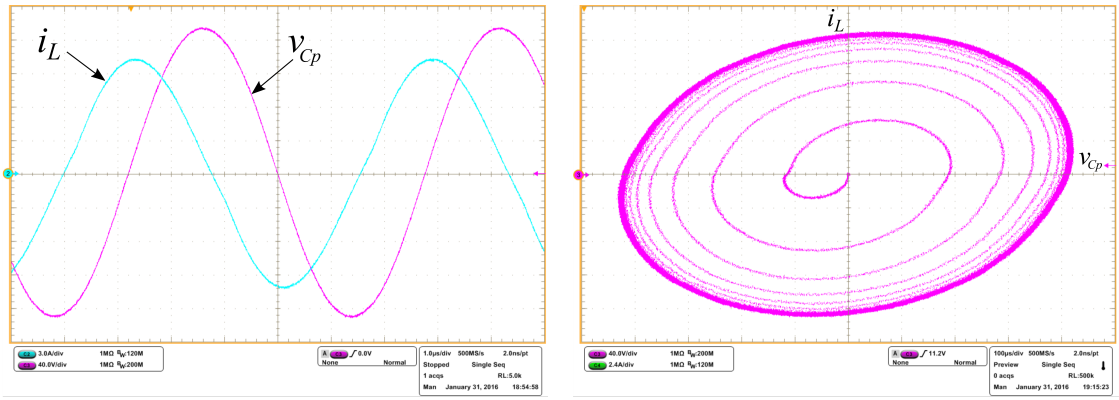

(**a**) (**b**)

Figure 8. Experimental waveforms of the self-oscillating LCC converter: (**a**) steady state current and voltage; (**b**) limit-cycle generation in the phase-plane $v_{Cp} - i_L$.

3.7. Stability Analysis

The mechanism of the ellipse generation consists in a spiral starting from zero initial conditions which finally converges into an ellipse. However, it should be ensured that such convergence always exists or equivalently the parametric conditions for such convergence should be found. With this purpose, the generation mechanism is described now by means of a discrete-time model as established by the zero current crossings in Figure 4b,c.

Taking into account the analysis made in Section 3.2, a generic T_{OFF} interval in Figure 4b,c can be described as

$$v_A(k) = -V_g(1 + e^{-\xi\pi}) + v_{Cs}(k)(1 - e^{-\xi\pi}) - v_{Cp}(k)e^{-\xi\pi} \tag{51}$$

$$v_B(k) = -V_g\frac{1 + e^{-\xi\pi}}{LC_s\omega_0^2} + v_{Cs}(k)\left(1 - \frac{1 + e^{-\xi\pi}}{LC_s\omega_0^2}\right) - v_{Cp}(k)\frac{1 + e^{-\xi\pi}}{LC_s\omega_0^2} \tag{52}$$

Moreover, the next T_{ON} interval will be characterized by

$$v_{Cs}(k+1) = V_g\frac{1 + e^{-\xi\pi}}{LC_s\omega_0^2} + v_B(k)\left(1 - \frac{1 + e^{-\xi\pi}}{LC_s\omega_0^2}\right) - v_A(k)\frac{1 + e^{-\xi\pi}}{LC_s\omega_0^2} \tag{53}$$

$$v_{Cp}(k+1) = V_g(1 + e^{-\xi\pi}) + v_B(k)(1 - e^{-\xi\pi}) - v_A(k)e^{-\xi\pi} \tag{54}$$

Introducing (51) and (52) in (53) and (54), the following discrete-time model can be obtained after simplification

$$\begin{pmatrix} v_{Cs}(k+1) \\ v_{Cp}(k+1) \end{pmatrix} = \begin{pmatrix} \phi_{11} & \phi_{12} \\ \phi_{21} & \phi_{22} \end{pmatrix}\begin{pmatrix} v_{Cs}(k) \\ v_{Cp}(k) \end{pmatrix} + \begin{pmatrix} \Gamma_1 \\ \Gamma_2 \end{pmatrix} V_g \tag{55}$$

The spiral will be stable if the eigenvalues of the discrete-time system (55) are located within the unit circle. The corresponding characteristic polynomial is given by $Q(\lambda) = \lambda^2 + b\lambda + c$, whose coefficients are:

$$b = \frac{-{K_C}^2 + 2 + 2K_C + 2K_Ce^{-\xi\pi} - (K_C + 2)^2e^{-2\xi\pi}}{(1 + K_C)^2} \tag{56}$$

$$c = \frac{(1 - K_Ce^{-\xi\pi})^2}{(1 + K_C)^2} \tag{57}$$

The eigenvalues will be located within the unit circle if the following conditions, derived from the application of Jury's criterion to a second order algebraic equation [36], are fulfilled:

1. $Q(1) > 0 \Rightarrow 1 + b + c > 0 \Rightarrow 1 > e^{-2\xi\pi}$
2. $Q(-1) > 0 \Rightarrow 1 - b + c > 0 \Rightarrow$
   $\Rightarrow {K_C}^2(1 + e^{-2\xi\pi}) + 2(1 + K_C)e^{-2\xi\pi} > 2K_C e^{-\xi\pi}$
3. $|c| < 1 \Rightarrow \left|1 - K_C e^{-\xi\pi}\right| < 1 + K_C$

It can be verified by simple inspection that conditions 1 and 3 are always satisfied. It can be also easily demonstrated that condition 2 is always fulfilled by substituting $x = e^{-\xi\pi}$, and observing that the function $g(x) = {K_C}^2(1 + x^2) + 2(1 + K_C)x^2 - 2K_C x$ is always positive. Therefore, it can be concluded that the generation of the spiral in the LCC self-oscillating resonant converter is always stable. Similarly, it can be noted that imposing $v_{Cs}(k+1) = v_{Cs}(k)$ and $v_{Cp}(k+1) = v_{Cp}(k)$ in (55) yields Equations (32) and (33), which corroborates the validity of the model.

4. 4th Order Self-Oscillating Resonant Converters

The approach described in the previous section can be directly applied to a LLC resonant converter (Figure 2d), but its extension to 4th order converters like the LCLC (Figure 2e) is apparently a difficult task. This is due to the complexity of the time-domain description of the 4th order differential equations involved. For that reason, the transient-state associated with each pole position is not exhaustively analyzed now but rather used as a conjecture to predict which poles are determinant in the generation of the limit cycle. In addition, the proved fact that the input impedance is resistive in the limit cycle will be used again to eventually establish the period of the resulting self-oscillating response.

Two different cases are now analyzed, they being characterized by the pole-zero diagrams depicted in Figure 9 and the constraint $L_s C_s = L_p C_p$. The first case in Figure 9a assumes the same natural oscillation frequency for the two pairs of complex conjugate poles while the second one in Figure 9b considers a big difference between the two natural oscillation frequencies.

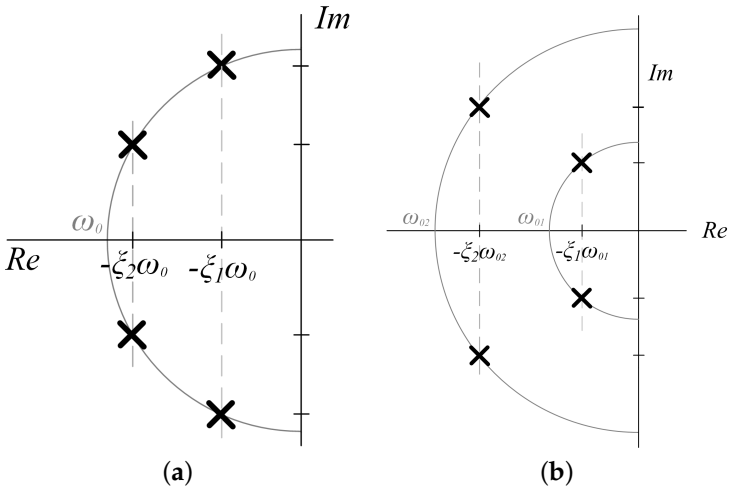

Figure 9. Pole-zero diagram of the proposed LCLC converter with: (**a**) $\omega_{02} = \omega_{01} = \omega_0$, (**b**) $\omega_{02} >> \omega_{01}$.

4.1. Equal Natural Oscillation Frequency

The analytical prediction lies in the following conjecture: If $\xi_2 >> \xi_1$ in Figure 9a, the self-oscillation will be determined by the complex conjugate pair $-\xi_1\omega_0 \pm j\omega_0\sqrt{1 - {\xi_1}^2}$.

Note that, in any T_{ON} or T_{OFF} subinterval, the time component associated with the pair of complex conjugate poles $-\xi_2\omega_0 \pm j\omega_0\sqrt{1 - {\xi_2}^2}$ will be much more damped than the one associated with the other pair of complex conjugate poles. It will exhibit a very low oscillating frequency, so that it will rapidly decrease to negligible positive values near zero but without crossing this threshold. Therefore, the zero crossings of input inductor current will be determined by the term associated with $-\xi_1\omega_0 \pm j\omega_0\sqrt{1 - {\xi_1}^2}$, which is significantly underdamped.

4.1.1. Parameter Identification

The input to output transfer function and input impedance of the LCLC resonant converter (Figure 2e) are given respectively by Equations (58) and (59):

$$H(s) = \left(\frac{s^2}{L_sC_p}\right) / \left(s^4 + \frac{s^3}{RC_p} + \left(\frac{1}{L_sC_s} + \frac{1}{L_pC_p} + \frac{1}{L_sC_p}\right)s^2 + \frac{s}{RC_pL_sC_s} + \frac{1}{L_pC_pL_sC_s}\right) \tag{58}$$

$$\begin{aligned} Z_i(s) = &\left(L_pL_sC_pC_sRs^4 + L_pL_sC_ss^3 + R(L_sC_s + L_pC_p\right. \\ &\left.+L_pC_s)s^2 + L_ps + R\right) / \left(C_s(L_pC_pRs^2 + L_ps + R)s\right) \end{aligned} \tag{59}$$

Expressing the normalized parameters ξ_1, ξ_2 and ω_0 of Figure 9a in terms of the converter parameters requires first equating the characteristic polynomial of the input–output transfer function of the LCLC to the normalized polynomial derived from the pole-zero diagram:

$$\begin{aligned} &s^4 + \frac{s^3}{RC_p} + \left(\frac{1}{C_s} + \frac{1}{C_p}\right)s^2 + \frac{s}{RC_pL_sC_s} + \frac{1}{L_pC_pL_sC_s} = \\ &= \left(s^2 + 2\xi_1\omega_{01}s + {\omega_{01}}^2\right)\left(s^2 + 2\xi_2\omega_{02}s + {\omega_{02}}^2\right) \end{aligned} \tag{60}$$

If $\omega_{02} = \omega_{01}$ is imposed in (60), it is found that

$${\omega_0}^4 = \frac{1}{L_pL_sC_pC_s} \tag{61}$$

In addition, since $L_sC_s = L_pC_p$, then

$${\omega_0}^2 = \frac{1}{L_sC_s} = \frac{1}{L_pC_p} \tag{62}$$

Introducing (62) and $s = j\omega_0$ into the input impedance transfer function $Zi(s)$ yields

$$Zi(j\omega_0) = R. \tag{63}$$

Thus, the behavior of the LCLC converter under these conditions is similar to the SRC, where the output is equal to the input at the resonant frequency.

In order to obtain the conditions for the existence of self-oscillation, a relationship between ξ_1 and ξ_2 has to be established. Identifying the coefficients in (60) leads to:

$$2(\xi_1 + \xi_2)\omega_0 = \frac{1}{C_pR} \tag{64}$$

$$2{\omega_0}^2(1 + 2\xi_1\xi_2) = \frac{2}{L_sC_s} + \frac{1}{L_sC_p} \tag{65}$$

$$2{\omega_0}^3(\xi_1 + \xi_2) = \frac{1}{L_sC_pC_sR} \tag{66}$$

Then, from (64), it is deduced that

$$\xi_1 + \xi_2 = \frac{1}{2C_pR\omega_0} \tag{67}$$

and from (65) it is obtained that

$$\xi_1\xi_2 = \frac{1}{4{\omega_0}^2L_sC_p} \tag{68}$$

From (67) and (68), it is derived:

$$\xi^2 - \frac{1}{2C_pR\omega_0}\xi + \frac{1}{4\omega_0{}^2L_sC_p} = 0 \tag{69}$$

$$\xi_{1,2} = \frac{1}{4C_pR\omega_0} \pm \frac{1}{4\omega_0}\sqrt{\frac{1}{C_p{}^2R^2} - \frac{4}{L_sC_p}}, \tag{70}$$

Therefore:

$$\frac{\xi_2}{\xi_1} = \frac{1}{2}\kappa\left(1 + \sqrt{1 - \frac{4}{\kappa}}\right) - 1\,, \tag{71}$$

where $\kappa = \frac{\frac{L_s}{C_p}}{R^2}$.

Thus, if $\kappa \geq 8$, then $\xi_2 \geq 5.82\,\xi_1$ and it can be assumed that the initial hypothesis on a large difference between damping factors holds.

4.1.2. Converter Design and Simulation Results

Taking into account the previous parameter identification, the design of a self-oscillating LCLC resonant converter acting as SRC can be simplified to an appropriate choice of the resonant tank elements according to the following steps:

1. Define the value of input voltage V_g.
2. Define the desired switching frequency ω_0 and the load R.
3. Select an arbitrary value of C_p.
4. Determine the value of κ given by $\kappa = \frac{L_s}{C_pR}$ and the constraint $\kappa \geq 8$.
5. Calculate the value of the series inductor L_s from $L_s = \kappa R^2C_p$
6. Calculate the value of the parallel inductor L_p from $L_p = \frac{1}{\omega_0{}^2C_p}$.
7. Calculate the value of the series capacitor C_s from $C_s = \frac{1}{\omega_0{}^2L_s}$.

As an example, a switching frequency of 160 kHz and a κ value of 10 are established for a load of $R = 100\,\Omega$ and a DC input voltage V_g of 12 V. Moreover, a parallel capacitor C_p of 10 nF is selected, leading to $L_s = 1$ mH, $L_p = 100\,\mu$H, $C_s = 1$ nF. The validity of the design is verified in the simulation of Figure 10, where the indexes of the depicted waveforms are in perfect agreement with the theoretical predictions, i.e., $v_{Cp,\,peak}$ = 15.3 V, $i_{Ls,\,peak}$ = 153 mA, $v_{Cs,\,peak}$ = 153.6 V and $i_{Lp,\,peak}$ = 153 mA and oscillation frequency of 160 kHz. It has to be pointed out that v_{Cs} and i_{Lp} are in phase exhibiting a phase-shift of -90° with respect to v_{Cp} and i_{Ls}, which, in turn, are in phase. This characteristic allows for representing the resulting four-dimensional limit cycle in a bi-dimensional plane just by adding the state-variables that are in phase. Thus, the following signals are associated taking into account the mentioned phase-shift among them:

$$x_1(t) = v_{Cp}(t) + i_{Ls}(t)(\times 1\Omega) \tag{72}$$

$$x_2(t) = v_{Cs}(t) + i_{Lp}(t)(\times 1\Omega) \tag{73}$$

This new representation method in a bi-dimensional plane facilitates the verification of the limit cycle generation in high-order converters. Figure 11 depicts the state-trajectory using this compact representation, for the previous simulation example. It can be seen that the proposed representation provides a convenient method to verify easily the correctness of a new design.

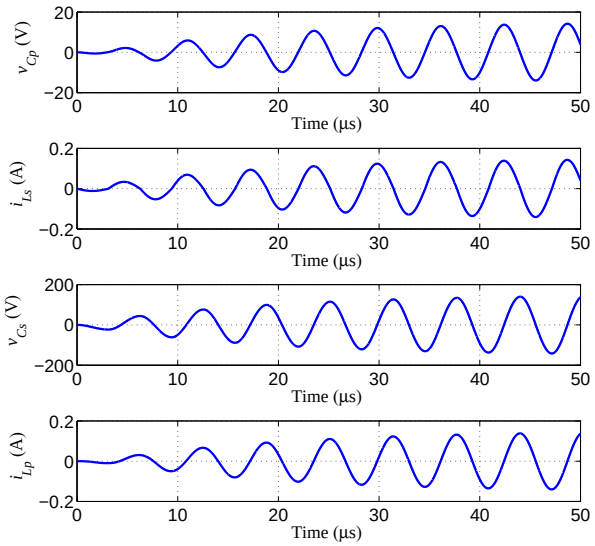

Figure 10. PSIM simulation of the time-domain waveforms of a self-oscillating resonant converter LCLC acting as SRC with $V_g = 12$ V, $f_0 = 160$ kHz, $\kappa = 10$, $R = 100\,\Omega$, $L_s = 1$ mH, $L_p = 0.1$ mH, $C_s = 1$ nF, $C_p = 10$ nF.

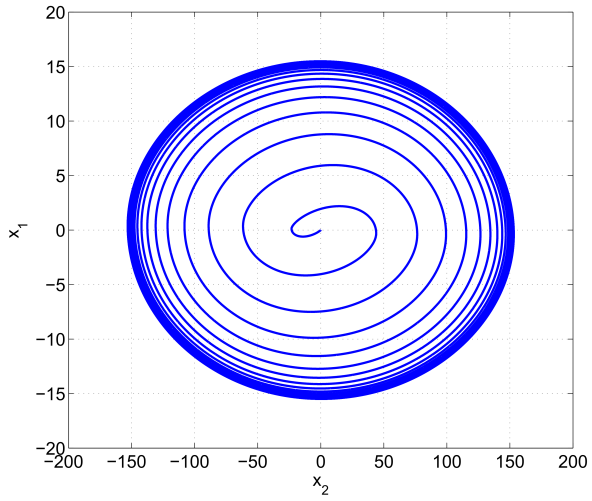

Figure 11. Matlab simulation of the compact representation of the limit cycle generation in the SRC-like LCLC.

4.2. Different Natural Oscillation Frequency

A second conjecture for the analytical predictions can be expressed as follows:

If $\omega_{02} >> \omega_{01}$ and $\xi_2\omega_{02} >> \xi_1\omega_{01}$ in Figure 9b, the self-oscillation will be determined by the complex conjugate pair $-\xi_2\omega_{02} \pm j\omega_{02}\sqrt{1-{\xi_2}^2}$.

Note that, in any T_{ON} or T_{OFF} subinterval, the time component associated with the pair of complex conjugate poles $-\xi_1\omega_{01} \pm j\omega_{01}\sqrt{1-{\xi_1}^2}$ will be less damped exhibiting a low oscillating frequency, so that it will be practically constant during the decay of the highly underdamped term created by $-\xi_2\omega_{02} \pm j\omega_{02}\sqrt{1-{\xi_2}^2}$, whose zero-crossings will establish the change from T_{ON} to T_{OFF} and vice versa.

4.2.1. Parameter Identification

Taking into account the design constraint $L_sC_s = L_pC_p$, the following identities can be obtained in (60):

$$\xi_2\omega_{02} = \frac{1}{2C_pR} \tag{74}$$

$$\omega_{02}{}^2 = \frac{2}{L_pC_p} + \frac{1}{L_sC_p} = \frac{2L_s + L_p}{L_sL_pC_p} \tag{75}$$

$$\omega_{01}{}^2\omega_{02}{}^2 = \frac{1}{L_p{}^2C_p{}^2} \tag{76}$$

$$2\xi_1\omega_{01}\omega_{02}{}^2 + 2\xi_2\omega_{02}\omega_{01}{}^2 = \frac{1}{L_pC_p{}^2R} \tag{77}$$

From (75) and (76), it can be deduced

$$\omega_{01}{}^2 = \frac{\frac{1}{L_p{}^2C_p{}^2}}{\omega_{02}{}^2} = \frac{L_s}{L_pC_p(2L_s + L_p)} \tag{78}$$

and, from (74), (75), (77) and (78), it is derived

$$\xi_1\omega_{01} = \frac{1}{2C_pR}\frac{L_s\left(L_s + L_p\right)}{\left(2L_s + L_p\right)^2} \tag{79}$$

Hence, from (74) and (79), we can write

$$\frac{\xi_2\omega_{02}}{\xi_1\omega_{01}} = \frac{\left(2L_s + L_p\right)^2}{L_s(L_s + L_p)} = \frac{\left(\frac{L_p}{L_s} + 2\right)^2}{\frac{L_p}{L_s} + 1} \tag{80}$$

Then, in order to satisfy the hypothesis $\xi_2\omega_{02} >> \xi_1\omega_{01}$, a minimum value of 7 for the ratio $\frac{L_p}{L_s}$ is required since for this value $\frac{\xi_2\omega_{02}}{\xi_1\omega_{01}} > 10$. Moreover, (75) and (78) yield

$$\frac{\omega_{02}{}^2}{\omega_{01}{}^2} = \frac{\left(2L_s + L_p\right)^2}{L_s{}^2} = \left(\frac{L_p}{L_s} + 2\right)^2 \tag{81}$$

Fulfillment of $\frac{\omega_{02}}{\omega_{01}} > 10$ in Equation (81) will be accomplished if $\frac{L_p}{L_s} > 8$. Consequently, denoting $L_p/L_s = K_l$, a value of K_l greater than 8 has to be selected in order to have self-oscillation with the predicted amplitude and frequency in this configuration.

On the other hand, introducing $L_pC_p = L_sC_s$ in Equation (59), the input impedance $Z_i(s)$ of the LCLC converter becomes:

$$Z_i(s) = L_p{}^2C_p{}^2 \cdot \frac{s^4 + \frac{s^3}{C_pR} + \left(\frac{2}{L_pC_p} + \frac{1}{L_sC_p}\right)s^2 + \frac{s}{L_pC_p{}^2R} + \frac{1}{L_p{}^2C_p{}^2}}{C_s\, s\left(1 + L_pC_ps^2 + \frac{L_p}{R}s\right)} \tag{82}$$

In addition, the assumption of self-oscillation due to the pair of poles $-\xi_2\omega_{02} \pm j\omega_{02}\sqrt{1 - \xi_2{}^2}$ suggests that the limit cycle will eventually present an oscillation frequency given by ω_{02}, as it was the case in 2nd and 3rd order converters. Therefore, the input impedance at that frequency must exhibit a resistive behavior.

Particularizing the input impedance at $s = j\omega_{02}$ yields after some manipulations

$$Z_i(j\omega_{02}) = \frac{RL_p}{C_s}\frac{K_l(K_l+2)}{(K_l+1)^2R^2+\frac{L_p}{C_p}(K_l+2)} + j\frac{K_l+1}{C_s\omega_{02}}\frac{R^2+\frac{L_p}{C_p}(K_l+2)}{(K_l+1)^2R^2+\frac{L_p}{C_p}(K_l+2)}, \tag{83}$$

which implies

$$\tan(\measuredangle Z_i(j\omega_{02})) = \frac{K_l+1}{\omega_{02}}\frac{R^2+\frac{L_p}{C_p}(K_l+2)}{RL_pK_l(K_l+2)} \tag{84}$$

On the other hand, from (75), it can be written

$$\omega_{02} = \sqrt{\frac{2L_s+L_p}{L_sL_pC_p}} = \sqrt{\frac{K_l+2}{L_pC_p}} \tag{85}$$

Hence, (84) becomes

$$\tan(\measuredangle Z_i(j\omega_{02})) = \frac{(K_l+1)}{K_l(K_l+2)^{\frac{3}{2}}}\left(Q_p + \frac{K_l+2}{Q_p}\right), \tag{86}$$

where $Q_p = \frac{R}{\sqrt{\frac{L_p}{C_p}}}$.

For a given value of K_l, the function $f(Q_p) = \left(Q_p + \frac{K_l+2}{Q_p}\right)$ has a minimum at

$$Q_{p,min} = \sqrt{K_l+2} \tag{87}$$

Therefore, the minimum value of (86) will be given by

$$min, \tan(\measuredangle Z_{in}(j\omega_{02})) = \frac{(K_l+1)2\sqrt{K_l+2}}{K_l(K_l+2)^{\frac{3}{2}}} = \frac{2(K_l+1)}{K_l(K_l+2)} \tag{88}$$

It can be observed from (88) that the phase-shift between input current and input voltage decreases monotonically to zero as K_l increases from its minimum value $K_l = 8$.

In addition, note that the value of the module of the input to output transfer function $H(s)$ given by (58) at the resonant frequency ($s = j\omega_{02}$) can be obtained approximately by means of the pole-zero diagram depicted in Figure 12. A very small damping factor ξ_2 is assumed, so that

$$\omega_{d2} \simeq \omega_{02} \tag{89}$$

As $\xi_2 << 1$, the modules of the vectors can be approximated by the length of their vertical cathetus. Therefore, $|D_1| = \xi_2\omega_{02}$, $|D_2| = 2\omega_{02}$, $|D_3| = \omega_{02} - \omega_{01}$, $|D_4| = \omega_{02} + \omega_{01}$ and $|N_1| = {\omega_{02}}^2$. Thus,

$$|H(j\omega_{02})| = \frac{K_l}{\sqrt{K_l+2}}Q_p\,. \tag{90}$$

For the minimum value of Q_p given by (87), Equation (90) becomes

$$|H(j\omega_{02})| = K_l \tag{91}$$

Since K_l must be bigger than 8, it can be concluded that the self-oscillating LCLC converter will operate as a high-gain voltage step-up stage.

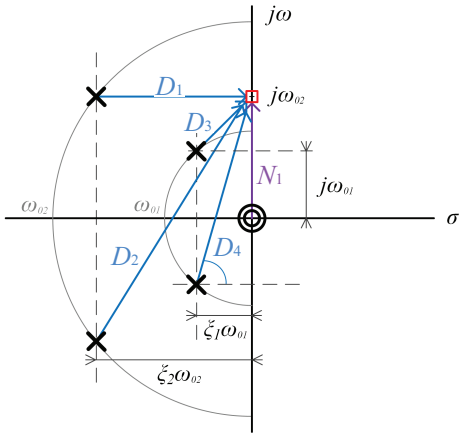

Figure 12. Pole-zero diagram of Figure 9b for evaluation of the input to output transfer function at $s = j\omega_{02}$.

4.2.2. Converter Design and Simulation Results

Considering the previous identification, the design steps of a self-oscillating LCLC resonant converter for high-gain voltage step-up operation can be summarized as follows:

1. Specify voltage gain K_l ($K_l > 8$), load resistance R and oscillation frequency ω_0.
2. Obtain the value of the parallel capacitor $C_p = \frac{K_l+2}{R\omega_0}$.
3. Calculate the value of the series capacitor $C_s = K_l C_p$.
4. Calculate the value of the parallel inductor $L_p = \frac{K_l+2}{\omega_0{}^2 C_p}$.
5. Determine the value of the series inductor $L_s = \frac{L_p}{K_l}$.

The design procedure is validated by the simulations illustrated in Figure 13a,b where a sinusoidal output voltage of 130 V amplitude and a frequency of 62 kHz is obtained for a load of 330 Ω and an input voltage of 12 V, which implies a voltage gain $K_l = 8.5$. The corresponding resonant tank parameters are C_p = 82 nF, C_s = 700 nF, L_p = 850 µH and L_s = 100 µH. Both the amplitude of the output voltage and the resulting oscillation frequency coincide with their respectively specified values. Like in the case of LCLC acting as SRC, the limit cycle generation can be described by a phase-plane compacted representation $x_1(t) - x_2(t)$ because capacitor voltages are in phase and inductor currents are out of phase, while both sets of signals are orthogonal. Hence, $x_1(t) = v_{Cp}(t) + v_{Cs}(t)$ and $x_2(t) = i_{Ls}(t) - i_{Lp}(t)$.

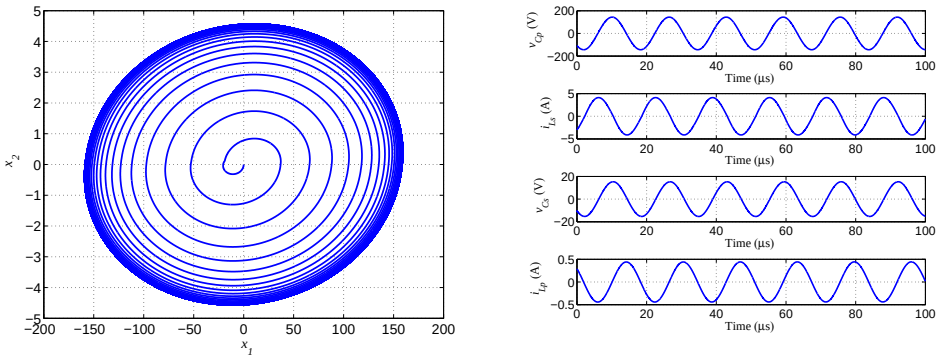

(**a**) (**b**)

Figure 13. Waveforms of the compact representation of the limit cycle generation in a voltage step-up LCLC self-oscillating resonant converter. The parameters of the converter are $V_g = 12$ V, $f_0 = 62$ kHz, $K_l = 8.5$ and $R = 330$ Ω: (**a**) Matlab simulation of the phase-plane trajectory ($x_1(t) = v_{Cp}(t) + v_{Cs}(t)$, $x_2(t) = i_{Ls}(t) - i_{Lp}(t)$); (**b**) Steady-state waveforms in a PSIM simulation.

5. Conclusions

The generation of the limit cycle in self-oscillating resonant converters employing the sign of the input inductor current to establish the change of topology has been proven to be effective in converters of 2nd, 3rd and 4th order. As a result, the input current and the first harmonic of the input voltage are in phase, which ensures a unity power factor to the steady-state operation of the resonant converter. This fact confers a nature of loss-free resistor to the two-port description of the converter.

In this context, predicting accurately the converter behavior in steady-state and deriving simple design rules to guarantee such behavior has required the assumption of several hypotheses on the converter parameters mainly related to big separation between poles and significant underdamping.

The hypotheses have allowed establishing a discrete recurrence considering two successive zero-crossings of the input inductor current after completing a generic oscillation cycle. The stability of the limit cycle generation has been demonstrated by proving the stability of the recurrence. This approach has successfully explained the generation of two-dimension and three-dimension spirals in 2nd and 3rd order converters respectively and has allowed determining the amplitude and period of the limit cycle at steady state by applying symmetry conditions.

The extension of the previous analytical procedure to 4th order converters has been interrupted by the complexity of the time-domain analysis involved. Instead, a conjecture on the dominant poles eventually provoking self-oscillation has been successfully used to predict the amplitude and period of the limit cycle in two different operation modes that share the same design constraint. The assumption about the dominant poles on the spiral generation has been analytically complemented by the fact that the input impedance is resistive at the oscillation frequency of the limit cycle.

Other steady-state solutions can be found empirically using the sign of the input inductor current to establish the change of topology in resonant converters but their exact analytical prediction is an open problem.

Author Contributions: L.M.-S. and C.O. conceptualized the research; L.M.-S. conceived the methodology and the formal analysis; R.B.-S. completed the investigation and carried out validation tasks; L.M.-S. and C.O. wrote the original draft; R.B.-S. and H.V.-B. reviewed and edited the final paper. All authors have read and agreed to the published version of the manuscript.

Funding: The research leading to these results has received funding from the spanish Agencia Estatal de Investigación under grants DPI2017-84572-C2-1-R, BES-2013-063288 and DPI2015-67292-R.

Conflicts of Interest: The authors declare no conflict of interest. The founding sponsors had no role in the design of the study; in the collection, analyses, or interpretation of data; in the writing of the manuscript, and in the decision to publish the results.

Abbreviations

The following abbreviations are used in this manuscript:

VSS	Variable structure system
PWM	Pulse-width modulated
SOPRC	Self-oscillating parallel resonant converter
SRC	Series resonant converter
PRC	Parallel resonant converter
LFR	Loss-free resistor

References

1. Kazimierczuk, M.; Czarkowski, D. *Resonant Power Converters*; John Wiley and Sons: Hoboken, NJ, USA, 2012.
2. Sebastian, J.; Rico, M.; Uceda, J.; Aldana, F. Regulated self-oscillating resonant converters. In Proceedings of the European Power Electronics Conference (EPE), Grenoble, France, 22–24 September 1987; pp. 245–249.
3. Kim, M.G.; Lee, D.S.; Youn, M.J. A new state feedback control of resonant converters. *IEEE Trans. Ind. Electron.* **1991**, *38*, 173–179. [CrossRef]

4. Rossetto, L. A simple control technique for series resonant converters. *IEEE Trans. Power Electron.* **1996**, *11*, 554–560. [CrossRef]
5. Pinheiro, H.; Jain, P.K.; Joos, G. Self-sustained oscillating resonant converters operating above the resonant frequency. *Power Electron. IEEE Trans.* **1999**, *14*, 803–815. [CrossRef]
6. Seidel, A.; Bisogno, F.; Pinheiro, H.; Do Prado, R.N. Self-oscillating dimmable electronic ballast. *IEEE Trans. Ind. Electron.* **2003**, *50*, 1267–1274. [CrossRef]
7. Youssef, M.Z.; Jain, P.K. A Novel Single Stage AC-DC Self-Oscillating Series-Parallel Resonant Converter. *IEEE Trans. Power Electron.* **2006**, *21*, 1735–1744. [CrossRef]
8. Gilbert, A.; Bingham, C.; Stone, D.; Foster, M. Self-oscillating control methods for the LCC current-output resonant converter. *IEEE Trans. Power Electron.* **2008**, *23*, 1973–1986. [CrossRef]
9. Williams, D.; Bingham, C.; Foster, M.; Stone, D. Hamel locus design of self-oscillating DC-DC resonant converters. *IET Power Electron.* **2010**, *3*, 86–94. [CrossRef]
10. Hsieh, J.C.; Lin, J.L. Novel single-stage self-oscillating dimmable electronic ballast with high power correction. *IEEE Trans. Ind. Electron.* **2011**, *58*, 250–262. [CrossRef]
11. Nerone, L.R. Autoswitching LED Driver. *IEEE Trans. Power Electron.* **2012**, *27*, 3834–3842. [CrossRef]
12. Cortés-Rodríguez, J.A.; Ponce-Silva, M. Self-Oscillating DC-DC Resonant Converter. In Proceedings of the 2012 IEEE Ninth Electronics, Robotics and Automotive Mechanics Conference, Cuernavaca, Mexico, 19–23 November 2012; pp. 300–304.
13. Yan, K.; Chen, Q.; Hou, J.; Ren, X.; Ruan, X. Self-Oscillating Contactless Resonant Converter With Phase Detection Contactless Current Transformer. *IEEE Trans. Power Electron.* **2014**, *29*, 4438–4449. [CrossRef]
14. Knott, A.; Andersen, T.M.; Kamby, P.; Pedersen, J.A.; Madsen, M.P.; Kovacevic, M.; Andersen, M.A.E. Evolution of Very High Frequency Power Supplies. *IEEE J. Emerg. Sel. Top. Power Electron.* **2014**, *2*, 386–394. [CrossRef]
15. Xu, L.; Chen, Q.; Ren, X.; Wong, S.C.; Tse, C.K. Self-Oscillating Resonant Converter With Contactless Power Transfer and Integrated Current Sensing Transformer. *IEEE Trans. Power Electron.* **2017**, *32*, 4839–4851. [CrossRef]
16. Oruganti, R.; Lee, F.C. Resonant Power Processors, Part I—State Plane Analysis. *IEEE Trans. Ind. Appl.* **1985**, *IA-21*, 1453–1460. [CrossRef]
17. Oruganti, R.; Lee, F.C. Resonant Power Processors, Part II—Methods of Control. *IEEE Trans. Ind. Appl.* **1985**, *IA-21*, 1461–1471. [CrossRef]
18. Glozman, S.; Ben-Yaakov, S. Dynamic interaction analysis of HF ballasts and fluorescent lamps based on envelope simulation. *IEEE Trans. Ind. Appl.* **2001**, *37*, 1531–1536. [CrossRef]
19. Yin, Y.; Zane, R.; Glaser, J.; Erickson, R.W. Small-signal analysis of frequency-controlled electronic ballasts. *IEEE Trans. Circuits Syst. Fundam. Theory Appl.* **2003**, *50*, 1103–1110. [CrossRef]
20. Sarnago, H.; Lucía, O.; Pérez-Tarragona, M.; Burdío, J.M. Dual-Output Boost Resonant Full-Bridge Topology and its Modulation Strategies for High-Performance Induction Heating Applications. *IEEE Trans. Ind. Electron.* **2016**, *63*, 3554–3561. [CrossRef]
21. Shakib, S.M.S.; Mekhilef, S. A Frequency Adaptive Phase Shift Modulation Control Based LLC Series Resonant Converter For Wide Input Voltage Applications. *IEEE Trans. Power Electron.* **2016**, *32*, 8360–8370. [CrossRef]
22. Sosa, J.L.; Castilla, M.; Miret, J.; de Vicuna, L.G.; Matas, J. Modeling and Performance Analysis of the DC/DC Series-Parallel Resonant Converter Operating With Discrete Self-Sustained Phase-Shift Modulation Technique. *IEEE Trans. Ind. Electron.* **2009**, *56*, 697–705. [CrossRef]
23. Mishima, T.; Takami, C.; Nakaoka, M. A new ZVS phase-shifted high-frequency resonant inverter incorporating asymmetrical PWM-based unit control for induction heating. In Proceedings of the IECON 2012—38th Annual Conference on IEEE Industrial Electronics Society, Montreal, QC, Canada, 25–28 October 2012; pp. 3256–3261.
24. Schnell, R.W.; Zane, R.A.; Azcondo, F.J. Size Reduction in Low-Frequency Square-Wave Ballasts for High-Intensity Discharge Lamps Using Soft-Saturation Magnetic Material and Digital Control Techniques. *IEEE Trans. Power Electron.* **2013**, *28*, 1036–1046. [CrossRef]
25. Zhou, S.; Li, X.; Zhong, Z.; Zhang, X. Wide ZVS operation of a semi-dual-bridge resonant converter under variable-frequency phase-shift control. *IET Power Electron.* **2020**, *13*, 1746–1755. [CrossRef]

26. Molla-Ahmadian, H.; Tahami, F.; Karimpour, A.; Naser, P. Hybrid control of DC-DC series resonant converters : The direct piecewise affine approach. *IEEE Trans. Power Electron.* **2015**, *30*, 1714–1736. [CrossRef]
27. Momeni, M.; Kelk, H.; Talebi, H. Rotating switching surface control of series-resonant converter based on a piecewise affine model. *IEEE Trans. Power Electron.* **2015**, *30*, 1762–1772. [CrossRef]
28. Afshang, H.; Tahami, F.; Molla-Ahmadian, H. Hybrid control of the DC-DC SRC operating below resonance. *IET Power Electron.* **2017**, *10*, 1–9. [CrossRef]
29. Namadmalan, A. Self-Oscillating Pulsewidth Modulation for Inductive Power Transfer Systems. *IEEE J. Emerg. Sel. Top. Power Electron.* **2020**, *8*, 1813–1820. [CrossRef]
30. Bonache-Samaniego, R.; Olalla, C.; Martinez-Salamero, L.; Valderrama-Blavi, H. Design of self-oscillating resonant converters based on a variable structure systems approach. *IET Power Electron.* **2016**, *9*, 111–119. [CrossRef]
31. Bonache-Samaniego, R.; Olalla, C.; Martínez-Salamero, L. Dynamic Modeling and Control of Self-Oscillating Parallel Resonant Converters Based on a Variable Structure Systems Approach. *IEEE Trans. Power Electron.* **2017**, *32*, 1469–1480. [CrossRef]
32. Singer, S. Realization of loss-free resistive elements. *IEEE Trans. Circuits Syst.* **1990**, *37*, 54–60. [CrossRef]
33. Singer, S. The application of loss-free resistors in power processing circuits. *IEEE Trans. Power Electron.* **1991**, *6*, 595–600. [CrossRef]
34. Katzir, L.; Singer, S.; Shmilovitz, D. Resonant converter with Loss Free Resistor Characteristic. In Proceedings of the 2005 IEEE 36th Power Electronics Specialists Conference, Recife, Brazil, 16 June 2005; pp. 656–659.
35. Bonache-Samaniego, R.; Olalla, C.; Martínez-Salamero, L.; Maksimović, D. 6.78 MHz self-oscillating parallel resonant converter based on GaN technology. In Proceedings of the 2017 IEEE Applied Power Electronics Conference and Exposition (APEC), Tampa, FL, USA, 26–30 March 2017; pp. 1594–1599.
36. Phillips, C.L.; Troy Nagle, H. *Digital Control Systems Analysis and Design*; Prentice-Hall International Editions: Upper Saddle River, NJ, USA, 1990.